WILEY | Hindawi

Research Article

Nonsingular Fast Terminal Sliding Mode Neural Network Decentralized Control of a Quadrotor Unmanned Aerial Vehicle

Yuqing Mao[1,2] and Jing Chen [ID][2]

[1]*Quzhou College of Technology, Quzhou 324000, China*
[2]*Jiangnan University, Wuxi 214122, China*

Correspondence should be addressed to Jing Chen; chenjing1981929@126.com

A nonsingular terminal sliding mode decentralized controller that can ensure the tracking errors of the trajectories and attitude rapid convergence in finite time is proposed for an insufficient driven and strongly coupled nonlinear four-rotor unmanned aerial vehicle (UAV). The total lift of the UAV system is decomposed into three virtual drive separation forces corresponding to the three positions. The insufficient drive UAV system is transformed into a virtual full-drive model for research. The three position states and the three attitude states of UAV are placed correspondingly to the six subsystems by variable substitution. The model uncertainty and unknown disturbance term for each subsystem serves as total coupling terms among the subsystems. The upper bounds of the total coupling terms are considered as unknown ordinary higher order polynomials varying with the six states of the system under the action of time change. With the help of Cauchy inequality, the estimates of the upper bounds are obtained from the approximation performance of the RBF neural network. Finally, the decentralized controller is designed for each attitude subsystem and the virtual decentralized controller for each position subsystem. It is also mapped to the tracking total lift controller by using the virtual decentralized position controller. The controller design process uses the nonsingular terminal sliding mode control technology to ensure that the quadrotor attitude and position variables can quickly converge to the desired value in a short time. Simulation experiments verify that the proposed control method is effective and feasible.

1. Introduction

1.1. Background. Being light sensitive and highly mobile, the quadrotor UAV can automatically perform tasks, such as image processing, video acquisition, environmental condition detection, site monitoring, and target tracking, which can be widely used in aerial photography, production supervision, public safety supervision, cargo distribution, combat reconnaissance, and other fields. The quadrotor UAV performs various missions by tracking the desired track. The accuracy of the tracking controller directly determines the quality of its task completion. However, the quadrotor is a complex nonlinear system with strong coupling, insufficient drive, multiple inputs, and multiple outputs. There is also a strong coupling effect between its posture and position. The task subjects to parameter uncertainty of the system and external environment interference, and all these factors greatly increase the difficulty of controller design.

1.2. Literature Review of Related Works. Recently, many scholars have proposed different effective control methods for tracking flight control problem of UAVs.

The authors of [1] presented a heuristic approach for optimal path planning that the optimization strategy is based on the indirect solution of the open-loop optimal control problem. In [2], a disturbance-observer-based adaptive fuzzy tracking control scheme is proposed for a medium-scale unmanned helicopter of six degrees of freedom in the presence of system uncertainties, flight boundary constraints, and external disturbances. In [3], a disturbance

observer is employed to estimate time-varying external disturbances and uncertainties for ducted fan aerial vehicles. The unknown disturbance is estimated as one of the unmeasured states based on the expansion state observer in [4–7].

The above literature uses different methods to solve the control problem of UAV affected by external disturbances. However, the UAV is a complex nonlinear system. For the complex nonlinear problem, literature [8] uses backstepping technology to design effective controllers.

In order to avoid the integral explosion problem in the backstepping control and to improve system robustness, the authors of [9] used the dynamic surface control method to design the controller. To solve the system uncertainty of the quadrotor, literature [4, 10–12] introduced the sliding mode control technology to design an adaptive sliding mode trajectory-tracking controller to compensate for model uncertainty and ensure the target-tracking performance. In literature [13], an event-triggered sliding mode solution is presented to reduce the update frequency of the control input and reduce the communication burden.

The above literature solves the problem of integral explosion of backstepping control by sliding mode control technology. However, the control process of the UAV usually needs to be achieved in a limited time, and attitude and position variables can achieve stability in a short time. Therefore, terminal sliding mode control methods are used in [14–19] literature.

In literature [14], a terminal sliding mode attitude-position quaternion based control of a quadrotor unmanned aerial vehicle is presented. In [15], robust nonlinear control strategies for attitude and position control are innovatively proposed based on a new continuous nonsingular terminal sliding mode control (CNTSMC) scheme. Literature [16] proposed a global fast terminal sliding mode controller for trajectory tracking. Literature [17] combines recursive control and robust control to design the finite-time adaptive integration reverse fast terminal sliding mode control method (FT-AIBFTSMC), which improves the external wind interference and unknown tracking performance by using virtual control laws and adaptive switch gain. In literature [18], a nonsingular fast terminal sliding mode control (NFTSMC) strategy based on a finite-time observer and an improved reaching rate is proposed to solve the control problem of aerial robot systems subject to actuator faults and internal and external disturbances. In [19], a new sliding mode surface-like variable-based position tracking control scheme and a novel nonsingular terminal sliding mode-based attitude synchronization control scheme are developed to drive the UAV tracking the reference trajectory with obstacle avoiding.

1.3. Contributions. Inspired by the above research, this paper is to solve control difficulty and complexity brought about by strong coupling. Quadrotor system uncertainties are affected by external time-varying perturbations during flight missions.

Because the radial-based function (RBF) neural network has global approximation ability, it can approximate any nonlinear function with arbitrary accuracy and has a simple structure and fast approximation speed, and we have designed a nonsingular fast sliding mode decentralized control method based on the radial fundamental neural network in this paper. The main contributions of this work are summarized as follows:

(1) Six interconnected subsystems were constructed from the three pose variables and three position variables. The uncertainty terms of each subsystem and external perturbations are discussed as lumped coupling terms between the subsystems. By considering that total coupling terms have upper bounds under time-varying action, and assuming that the upper bounds are unknown, ordinary higher order polynomials about the six state-tracking errors of the quadrotor, the estimates are obtained by using the deformation of the Cauchy inequality and the approximation power of the RBF neural network.

(2) To overcome the strong coupling effect between pose subsystems, pose decentralized controllers are designed so that any attitude controller is related to none of the other two poses and the three position variables but only the corresponding pose variable. When the quadrotor attitude is deflected on a certain space surface, we can adjust only the attitude angle on the corresponding space surface to achieve the desired control effect, which greatly reduces control difficulty caused by the mutual coupling of the subsystems. In the design of the attitude decentralized controller, position virtual decentralized controllers are also designed. The total lift controller is finally obtained according to the mapping relationship between the position virtual controller and the total lift. Then, the angular speed controllers of the four rotors are obtained.

(3) In order to ensure that quadrotor attitude and position variables can quickly converge to the expected value in a short time, nonsingular terminal sliding mode control technology is used in the controller design process. The Lyapunov theory proves the stability of the system, and the simulation experiment verifies that the proposed control method is effective and feasible.

The rest of this paper is organized as follows: Section 2 details the modeling and problem description of the UAV system. Section 3 shows the controller design. Section 4 shows the stability analysis. Simulation results are presented in Section 5 to demonstrate the effectiveness of the proposed control scheme. Finally, the article is summarized in Section 6.

Remark 1. Existing works in the literature have proposed and implemented sliding mode controllers on real quadrotor hardware. Considering that the actual UAV is sometimes

implemented for new kinds of mission in which unmodeled dynamics or disturbances are present, so as future directions, these control strategies will be extended for systems with unmodeled dynamics and uncertainties.

2. Problem Statement

The structure of the quadrotor UAV consists mainly of "+" and "X" types. In this paper, an "X" quadrotor UAV is studied. The specific structure and motion state are shown in Figure 1. The four motors of the quadrotor provide power, and the motor speed change controls the rotor speed change; thus, the three positions of front and back, left and right, up and down, as well as the three poses of pitch, roll, and yaw are adjusted. The coordinate origin of the ground coordinate system is the take-off point of the UAV, and the coordinate origin of the body coordinate system is the geometric center of the four rotors of the UAV. According to the Newtonian acceleration formula and the Newton–Euler theorem of motion, the kinetic model of a quadrotor UAV can be described by the following equations which are obtained under the "small angle approximation" assumption [14]:

$$
\ddot{x} = \frac{1}{m}(\cos\varphi\sin\theta\cos\psi + \sin\varphi\sin\psi)u_h - \frac{1}{m}l_1\dot{x} + \frac{1}{m}d_1,
$$

$$
\ddot{y} = \frac{1}{m}(\cos\varphi\sin\theta\sin\psi - \sin\varphi\cos\psi)u_h - \frac{1}{m}l_2\dot{y} + \frac{1}{m}d_2,
$$

$$
\ddot{z} = \frac{1}{m}(\cos\varphi\cos\theta)u_h - g - \frac{1}{m}l_3\dot{z} + \frac{1}{m}d_3,
$$

$$
\ddot{\varphi} = \dot{\theta}\dot{\psi}\frac{I_y - I_z}{I_x} + \frac{J_r}{I_x}\dot{\theta}\Omega_r + \frac{l}{I_x}u_\varphi - \frac{1}{I_x}l_4 l\dot{\varphi} + d_4,
$$

$$
\ddot{\theta} = \dot{\psi}\dot{\varphi}\frac{I_z - I_x}{I_y} - \frac{J_r}{I_y}\dot{\varphi}\Omega_r + \frac{l}{I_y}u_\theta - \frac{1}{I_y}l_5 l\dot{\theta} + d_5,
$$

$$
\ddot{\psi} = \dot{\varphi}\dot{\theta}\frac{I_x - I_y}{I_z} + \frac{1}{I_z}u_\psi - \frac{1}{I_z}l_6\dot{\psi} + d_6.
$$

$$(1)$$

Here, $\Omega_r = \omega_1 - \omega_2 + \omega_3 - \omega_4$. The mapping between $u_h, u_\varphi, u_\theta, u_\psi$ and $\omega_1, \omega_2, \omega_3, \omega_4$ is shown in formula (3):

$$
\begin{cases}
u_h = b\left(\omega_1^2 + \omega_2^2 + \omega_3^2 + \omega_4^2\right), \\[2mm]
u_\varphi = b\left(\omega_4^2 - \omega_2^2\right), \\[2mm]
u_\theta = b\left(-\omega_1^2 + \omega_3^2\right), \\[2mm]
u_\psi = \frac{d}{b}\left(-\omega_1^2 + \omega_2^2 - \omega_3^2 + \omega_4^2\right),
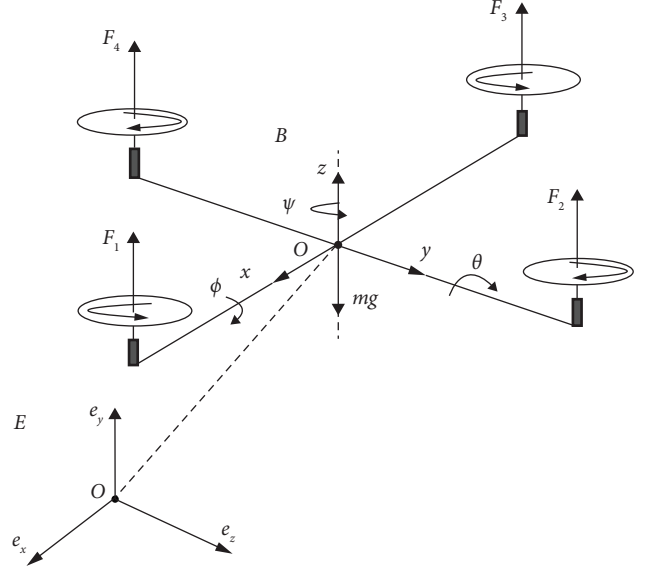\end{cases}
$$

$$(2)$$

that is,

FIGURE 1: Working principle of a four-rotor UAV.

$$
\begin{cases}
\omega_1 = \sqrt{b\left(\frac{1}{4}u_h - \frac{1}{2}u_\theta - \frac{1}{4}u_\psi\right)}, \\[3mm]
\omega_2 = \sqrt{b\left(\frac{1}{4}u_h - \frac{1}{2}u_\varphi + \frac{1}{4}u_\psi\right)}, \\[3mm]
\omega_3 = \sqrt{b\left(\frac{1}{4}u_h + \frac{1}{2}u_\theta - \frac{1}{4}u_\psi\right)}, \\[3mm]
\omega_4 = \sqrt{\frac{d}{b}\left(\frac{1}{4}u_h + \frac{1}{2}u_\theta + \frac{1}{4}u_\psi\right)}.
\end{cases}
$$

$$(3)$$

Here, b, d are the lift coefficient and force to torque scale factor of the rotor, respectively.

To achieve attitude decentralized control, the three positions and three attitude angles of the UAV are considered as states corresponding to the six subsystems, represented by six-dimensional vectors, which are

$$
\underline{\mathbf{x}}_1 = \left(x_{11}, x_{21}, x_{31}, x_{41}, x_{51}, x_{61}\right)^T = (x, y, z, \varphi, \theta, \psi)^T. \quad (4)
$$

The first derivative of the subsystem vector is denoted as $\underline{\mathbf{x}}_2$, which is

$$
\underline{\mathbf{x}}_2 = \left(x_{12}, x_{22}, x_{32}, x_{42}, x_{52}, x_{62}\right)^T = (\dot{x}, \dot{y}, \dot{z}, \dot{\varphi}, \dot{\theta}, \dot{\psi})^T. \quad (5)
$$

$\underline{\mathbf{d}} = (d_1, d_2, d_3, d_4, d_5, d_6)^T$ is the external time-varying disturbance of the subsystem.

$\underline{\mathbf{y}}_d = (y_{d1}, y_{d2}, y_{d3}, y_{d4}, y_{d5}, y_{d6})^T = (x_d, y_d, z_d, \varphi_d, \theta_d, \psi_d)^T$ is the expected tracking trajectory of each subsystem. The quadrotor UAV system described in equation (1) can be converted into the following model:

$$
\begin{cases}
\dot{x}_{i1} = x_{i2}, \\
\dot{x}_{i2} = u_i + \Delta_i.
\end{cases}
$$

$$(6)$$

Here, $u_i (i = 1 \cdots 6)$ are the control inputs to each subsystem of the system, $\Delta_i (i = 1 \cdots 6)$ are the total coupling terms of each subsystem composed of external perturbations, model uncertainty, and strong coupling terms between the subsystems, and they are given by formulas (7) and (8), respectively:

$$u_1 = \frac{\cos \varphi \sin \theta \cos \psi + \sin \varphi \sin \psi}{m} u_h,$$

$$u_2 = \frac{\cos \varphi \sin \theta \sin \psi - \sin \varphi \cos \psi}{m} u_h,$$

$$u_3 = \frac{\cos \varphi \cos \theta}{m} u_h,$$

$$u_4 = \frac{l}{I_x} u_\varphi, \qquad (7)$$

$$u_5 = \frac{l}{I_y} u_\theta,$$

$$u_6 = \frac{1}{I_z} u_\psi,$$

$$\Delta_1 = -\frac{1}{m} l_1 x_{12} + \frac{1}{m} d_1,$$

$$\Delta_2 = -\frac{1}{m} l_2 x_{22} + \frac{1}{m} d_2,$$

$$\Delta_3 = -g - \frac{1}{m} l_3 x_{32} + \frac{1}{m} d_3,$$

$$\Delta_4 = \frac{I_y - I_z}{I_x} x_{52} x_{62} + \frac{J_r}{I_x} x_{52} \Omega_r - \frac{1}{I_x} l_4 l x_{42} + d_4,$$

$$\Delta_5 = \frac{I_z - I_x}{I_y} x_{42} x_{62} - \frac{J_r}{I_y} x_{42} \Omega_r - \frac{1}{I_y} l_5 l x_{52} + d_5,$$

$$\Delta_6 = \frac{I_x - I_y}{I_z} x_{42} x_{52} - \frac{1}{I_z} l_6 x_{62} + d_6.$$

$$(8)$$

In this paper, the attitude decentralized controllers named u_4, u_5, u_6 and the position decentralized virtual controllers named u_1, u_2, u_3 are designed for the strongly coupled four-rotor UAV described in (1)–(8), and then, the total lift control law is obtained through the mapping relationship of (8).

3. Controller Design

The trajectory-tracking error of each subsystem of the quadrotor UAV is described by

$$\begin{cases} e_{i1} = x_{i1} - y_{di}, \\ e_{i2} = x_{i2} - \dot{y}_{di}. \end{cases} (i = 1 \cdots 6). \qquad (9)$$

Here, $\underline{e}_i = (e_{i1}, e_{i2})^T$ is the model (6) that can be changed into the following formula:

$$\begin{cases} \dot{e}_{i1} = e_{i2}, \\ \dot{e}_{i2} = u_i + \Delta_i - \ddot{y}_{di}. \end{cases} \qquad (10)$$

Then, the nonsingular sliding mode surface of each subsystem is shown in the following formula:

$$s_i = e_{i1} + \frac{1}{a_i} e_{i1}^{(k_i/h_i)} + \frac{1}{b_i} \dot{e}_{i1}^{(p_i/q_i)}, \ (i = 1, \ldots, 6) \qquad (11)$$

Here, $a_i, b_i > 0$ and k_i, h_i, p_i, q_i are all in positive and odd numbers, and $1 < p_i/q_i < 2, p_i/q_i < k_i/h_i$.

In order to easily represent the relationship of the variables in the controller design process, the following assumptions are made on the system-related variables.

Hypothesis 2. The total coupling terms of each subsystem are bounded, and the upper bounds are unknown, ordinary higher order polynomials for the six state-tracking errors corresponding to the UAV position and attitude, i.e.,

$$|\Delta_i| \le \sum_{k=0}^{M} \sum_{j=1}^{6} c_{ijk} \left(|e_{j1}|^k + |e_{j2}|^k \right). \qquad (12)$$

Hypothesis 3. The expected trajectory of each subsystem and its first and second-order derivatives are bounded; that is, the existence of $Y_{di} > 0$ can make the following inequalities hold true:

$$|y_{di}| \left(|\dot{y}_{di}|, |\ddot{y}_{di}| \right) \le Y_{di}. \qquad (13)$$

Theorem 4. *According to the dynamic model, the tracking error for the six subsystems of the three position variables and the three pose variables of a quadrotor robot is shown in formula (10), the fast nonsingular terminal sliding mode controllers are shown in formula (14), and the parameter adaptive laws shown in formulas (15) and (16) are designed, respectively, to ensure that the tracking error of each subsystem converges in a finite time:*

$$u_i = -s_i - \left(1 + \frac{k_i}{a_i h_i} e_{i1}^{((k_i/h_i)-1)} \right) \frac{b_i q_i}{p_i} \dot{e}_{i1}^{(2-(p_i/q_i))} - \frac{s_i p_i}{4 b_i q_i} \dot{e}_{i1}^{((p_i/q_i)-1)}$$

$$- \text{sat}(s_i) Y_{di} - \text{sat}(s_i) \frac{b_i q_i}{p_i \left(\dot{e}_{i1}^{(p_i/q_i - 1)} - \eta_i \right)} \widehat{\varepsilon}_i$$

$$- \text{sat}(s_i) \frac{b_i q_i}{I p_i \left(\dot{e}_{i1}^{((p_i/q_i)-1)} - \eta_i \right)} \widehat{\mathbf{W}}_i^T \boldsymbol{\zeta}_i,$$

$$(14)$$

$$\dot{\widehat{\mathbf{W}}}_i = \begin{cases} r_i |s_i| \underline{\boldsymbol{\zeta}}_i(\underline{\mathbf{e}}_i) & \text{when } \left\| \widehat{\mathbf{W}}_i \right\| < M_{W_i}, \\ \quad \text{or } \left\| \widehat{\mathbf{W}}_i \right\| = M_{W_i}, \widehat{\mathbf{W}}_i^T \boldsymbol{\zeta}_i(\underline{\mathbf{e}}_i) \le 0, \\ r_i \left(|s_i| \underline{\boldsymbol{\zeta}}_i(\underline{\mathbf{e}}_i) - |s_i| \frac{\widehat{\mathbf{W}}_i \widehat{\mathbf{W}}_i^T}{\left\| \widehat{\mathbf{W}}_i \right\|^2} \boldsymbol{\zeta}_i(\underline{\mathbf{e}}_i) \right), \\ \quad \text{when } \left\| \widehat{\mathbf{W}}_i \right\| = M_{W_i} \text{ and } \widehat{\mathbf{W}}_i^T \boldsymbol{\zeta}_i(\underline{\mathbf{e}}_i) > 0. \end{cases} \qquad (15)$$

$$\dot{\widehat{\varepsilon}}_i = \begin{cases} \tau_i |s_i| & \text{when } |\widehat{\varepsilon}_i| < M_{\varepsilon_i}, \\ & \text{or } |\widehat{\varepsilon}_i| = M_{\varepsilon_i}, \widehat{\varepsilon}_i \le 0, \\ 0 & \text{when } |\widehat{\varepsilon}_i| = M_{\widehat{\varepsilon}_i}, \widehat{\varepsilon}_i > 0. \end{cases} \tag{16}$$

Here, $r_i, \tau_i > 0$ are the parametric adaptive rates, $M_{W_i}, M_{\widehat{\varepsilon}_i} > 0, \eta_i > 2$ are the design constants, and I is a design value.

$$I = \begin{cases} 1, & \text{when } \underline{\widehat{W}}_i^T \zeta_i \ge 0, \\ \dfrac{1}{\dot{e}_{i1}^{((p_i/q_i)-1)} - \eta_i}, & \text{when } \underline{\widehat{W}}_i^T \zeta_i < 0. \end{cases} \tag{17}$$

$$\text{sat}(s_i) = \begin{cases} s_i, & |s_i| \le 1, \\ \text{sgn}(s_i), & |s_i| > 1. \end{cases} \tag{18}$$

Remark 5. As can be seen from the controllers given by equation (14), the controllers of the three quadrotor attitude variables are only related to each attitude variable itself, which greatly improves the control performance.

Remark: As existing works shown in literature [12], the saturation function can be used to eliminate shaking vibration when to realize sliding mode controllers in practice. Since in the sliding mode control, the value of the switching control function is in the boundary layer for most of the time, and the feedback control rather than the switching control is used in the control law, so the vibration is well suppressed.

4. Stability Analysis

k_i, h_i, p_i, q_i are all positive and odd, and $1 < p_i/q_i < 2, p_i/q_i < k_i/h_i$ so $\dot{e}_{i1}^{p_i/q_i - 1} \ge 0$. The Lyapunov function of the i-th subsystem can be defined as

$$V_i = \frac{1}{2} s_i^2 + \frac{1}{2r_i} \widetilde{W}_i^T \widetilde{W}_i + \frac{1}{2\tau_i} \widetilde{\varepsilon}_i^2. \tag{19}$$

The derivative of equation (19) is given by

$$\begin{aligned} \dot{V}_i &= s_i \dot{s}_i - \frac{1}{r_i} \widetilde{W}_i^T \dot{\widehat{W}}_i - \frac{1}{\tau_i} \widetilde{\varepsilon}_i \dot{\widehat{\varepsilon}}_i \\ &= s_i \left(\dot{e}_{i1} + \frac{k_i}{a_i h_i} e_{i1}^{((k_i/h_i)-1)} \dot{e}_{i1} + \frac{p_i}{b_i q_i} \dot{e}_{i1}^{((p_i/q_i)-1)} \ddot{e}_{i1} \right) \\ &\quad - \frac{1}{r_i} \widetilde{W}_i^T \dot{\widehat{W}}_i - \frac{1}{\tau_i} \widetilde{\varepsilon}_i \dot{\widehat{\varepsilon}}_i \\ &= s_i \dot{e}_{i1} \left(1 + \frac{k_i}{a_i h_i} e_{i1}^{((k_i/h_i)-1)} \left(+\frac{s_i p_i}{b_i q_i} \dot{e}_{i1}^{((p_i/q_i)-1)} \right) u_i + \Delta_i - \ddot{y}_{di} \right) \\ &\quad - \frac{1}{r_i} \widetilde{W}_i^T \dot{\widehat{W}}_i - \frac{1}{\tau_i} \widetilde{\varepsilon}_i \dot{\widehat{\varepsilon}}_i. \end{aligned} \tag{20}$$

Here, $a_i, b_i > 0$ and k_i, h_i, p_i, q_i are all positive and odd, and $1 < p_i/q_i < 2, p_i/q_i < k_i/h_i \dot{e}_{i1}^{p_i/q_i-1}, e_{i1}^{k_i/h_i-1} > 0$, so we can get the derivative of V_i shown by

$$\begin{aligned} \dot{V}_i &\le s_i \dot{e}_{i1} \left(1 + \frac{k_i}{a_i h_i} e_{i1}^{((k_i/h_i)-1)} \right) + \frac{s_i p_i}{b_i q_i} \dot{e}_{i1}^{((p_i/q_i)-1)} u_i \\ &\quad + \frac{s_i^2 p_i^2}{4 b_i^2 q_i^2} \dot{e}_{i1}^{2((p_i/q_i)-1)}, \\ &\quad + \frac{|s_i| p_i}{b_i q_i} \dot{e}_{i1}^{((p_i/q_i)-1)} Y_{di} + \Delta_i^2 - \frac{1}{r_i} \widetilde{W}_i^T \dot{\widehat{W}}_i - \frac{1}{\tau_i} \widetilde{\varepsilon}_i \dot{\widehat{\varepsilon}}_i. \end{aligned} \tag{21}$$

The Lyapunov function defining the quadrotor UAV system is given by

$$V = \sum_{i=1}^{6} V_i. \tag{22}$$

The derivative of equation (22) is given by

$$\begin{aligned} \dot{V} &= \sum_{i=1}^{6} \dot{V}_i \\ &\le \sum_{i=1}^{6} \left[s_i \dot{e}_{i1} \left(1 + \frac{k_i}{a_i h_i} e_{i1}^{((k_i/h_i)-1)} \right) + \frac{s_i p_i}{b_i q_i} \dot{e}_{i1}^{((p_i/q_i)-1)} u_i + \frac{s_i^2 p_i^2}{4 b_i^2 q_i^2} \dot{e}_{i1}^{2((p_i/q_i)-1)} \right. \\ &\quad \left. + \frac{|s_i| p_i}{b_i q_i} \dot{e}_{i1}^{((p_i/q_i)-1)} Y_{di} + \Delta_i^2 - \frac{1}{r_i} \widetilde{W}_i^T \dot{\widehat{W}}_i - \frac{1}{\tau_i} \widetilde{\varepsilon}_i \dot{\widehat{\varepsilon}}_i \right] \\ &\le \sum_{i=}^{6} \left[s_i \dot{e}_{i1} \left(1 + \frac{k_i}{a_i h_i} e_{i1}^{((k_i/h_i)-1)} \right) + \frac{s_i p_i}{b_i q_i} \dot{e}_{i1}^{((p_i/q_i)-1)} u_i \right. \end{aligned}$$

$$
\begin{aligned}
& + \frac{s_i^2 p_i^2}{4b_i^2 q_i^2} \dot{e}_{i1}^{2((p_i/q_i)-1)} + \frac{|s_i| p_i}{b_i q_i} \dot{e}_{i1}^{((p_i/q_i)-1)} Y_{\mathrm{di}} - \frac{1}{r_i} \widetilde{\mathbf{W}}_{\mathbf{i}}^{\mathbf{T}} \hat{\mathbf{W}}_{\mathbf{i}} - \frac{1}{\tau_i} \widetilde{\varepsilon}_i \hat{\varepsilon}_i \Bigg] \\
& + \sum_{i=1}^{6} \left[\sum_{k=0}^{M} \sum_{j=1}^{6} c_{ijk} \left(\left| e_{j1} \right|^k + \left| e_{j2} \right|^k \right) \right]^2 \\
& \leq \sum_{i=}^{6} \Bigg[s_i \dot{e}_{i1} \left(1 + \frac{k_i}{a_i h_i} e_{i1}^{((k_i/h_i)-1)} \right) + \frac{s_i p_i}{b_i q_i} \dot{e}_{i1}^{((p_i/q_i)-1)} u_i \\
& + \frac{s_i^2 p_i^2}{4b_i^2 q_i^2} \dot{e}_{i1}^{2((p_i/q_i)-1)} + \frac{|s_i| p_i}{b_i q_i} \dot{e}_{i1}^{((p_i/q_i)-1)} Y_{\mathrm{di}} - \frac{1}{r_i} \widetilde{\mathbf{W}}_{\mathbf{i}}^{\mathbf{T}} \hat{\mathbf{W}}_{\mathbf{i}} - \frac{1}{\tau_i} \widetilde{\varepsilon}_i \hat{\varepsilon}_i \Bigg] \\
& + 6(\mathrm{M}+1)^2 \sum_{i=1}^{6} \sum_{k=0}^{M} \sum_{j=1}^{6} c_{ijk}^2 \left(\left| e_{j1} \right|^k + \left| e_{j2} \right|^k \right)^2 .
\end{aligned}
\tag{23}
$$

Let $f_{ijk}(e_{j1}, e_{j2}) = \sum_{j=1}^{6} c_{ijk}^2 (|e_{j1}|^k + |e_{j2}|^k)^2$, and if $|s_j| > \mu > 1$, then

$$
\begin{aligned}
& 6(\mathrm{M}+1)^2 \sum_{i=1}^{6} \sum_{k=0}^{M} \sum_{j=1}^{6} c_{ijk}^2 \left(\left| e_{j1} \right|^k + \left| e_{j2} \right|^k \right)^2 \\
& \leq 6(\mathrm{M}+1)^2 \sum_{i=1}^{6} \sum_{k=0}^{M} \sum_{j=1}^{6} f_{ijk}(e_{j1}, e_{j2}) |s_j| \\
& \leq \sum_{i=1}^{6} |s_i| 6(\mathrm{M}+1)^2 \sum_{k=0}^{M} \left(f_{1ik}(e_{i1}, e_{i2}) + \cdots + f_{6ik}(e_{i1}, e_{i2}) \right).
\end{aligned}
\tag{24}
$$

Let

$$
D_i(e_{i1}, e_{i2}) = 6(\mathrm{M}+1)^2 \sum_{k=0}^{M} \left(f_{1ik}(e_{i1}, e_{i2}) + \cdots + f_{6ik}(e_{i1}, e_{i2}) \right),
\tag{25}
$$

where $D_i(e_{i1}, e_{i2})$ are continuous functions. Therefore, the approximation can be performed with radial-based neural networks, i.e.,

$$
D_i(e_{i1}, e_{i2}) = \underline{\mathbf{W}}_i^{*T} \underline{\zeta}_i(\underline{\mathbf{e}}_i) + \varepsilon_i(\underline{\mathbf{e}}_i).
\tag{26}
$$

Here, $\underline{\mathbf{e}}_i = [e_{i1}, e_{i2}]^T \in R^2$ is the input signal of a neural network, $\underline{\mathbf{W}}_i^* = (\mathbf{w}_{1i}, \mathbf{w}_{2i}, \cdots, \mathbf{w}_{mi})^T$ is the optimal weight of the neural network, $\hat{\mathbf{W}}_{\mathbf{i}}$ is the estimate of $\underline{\mathbf{W}}_i^*$, and $\widetilde{\mathbf{W}} = \underline{\mathbf{W}}_i^* - \hat{\mathbf{W}}.$

$\underline{\zeta}_i(\underline{\mathbf{e}}_i) = [\zeta_{i1}(\underline{\mathbf{e}}_i), \zeta_{i2}(\underline{\mathbf{e}}_i), \cdots, \zeta_{im}(\underline{\mathbf{e}}_i)]^T \in R^m$ are Gaussian-type basis functions, where $\zeta_{ij}(\underline{\mathbf{e}}_i) = \exp[-(\underline{\mathbf{e}}_i - \sigma_{ij})^T (\underline{\mathbf{e}}_i - \sigma_{ij})/c_{ij}^2]$ and σ_{ij}, c_{ij} are, respectively, center and basis width parameters of the j-th neuron basis function in the hidden layer, $\varepsilon_i(\underline{\mathbf{e}}_i)$ is the approximation error of the neural network, and $\exists \varepsilon_i > 0$, $|\varepsilon_i(\underline{\mathbf{e}}_i)| \leq \varepsilon_i$, and $\hat{\varepsilon}_i > 0$ are the estimates of ε_i and $\widetilde{\varepsilon}_i = \varepsilon_i - \hat{\varepsilon}_i.$ The neural network model for approximating the continuous function is shown in Figure 2.

Thus,

$$
\begin{aligned}
\dot{V} \leq \sum_{i=1}^{6} \Bigg[& s_i \dot{e}_{i1} \left(1 + \frac{k_i}{a_i h_i} e_{i1}^{(k_i/h_i)-1} \right) + \frac{s_i p_i}{b_i q_i} \dot{e}_{i1}^{(p_i/q_i)-1} u_i + \frac{s_i^2 p_i^2}{4b_i^2 q_i^2} \dot{e}_{i1}^{2((p_i/q_i)-1)} \\
& + \frac{|s_i| p_i}{b_i q_i} \dot{e}_{i1}^{(p_i/q_i)-1} Y_{\mathrm{di}} + |s_i| \underline{\mathbf{W}}_i^{*T} \underline{\zeta}_i(\underline{\mathbf{e}}_i) + |s_i| \varepsilon_i - \frac{1}{r_i} \widetilde{\mathbf{W}}_{\mathbf{i}}^{\mathbf{T}} \dot{\hat{\mathbf{W}}}_{\mathbf{i}} - \frac{1}{\tau_i} \widetilde{\varepsilon}_i \dot{\hat{\varepsilon}}_i \Bigg] \\
\leq \sum_{i=1}^{6} \Bigg[& -\frac{p_i}{b_i q_i} \dot{e}_{i1}^{(p_i/q_i)-1} s_i^2 - |s_i| \frac{\dot{e}_{i1}^{(p_i/q_i)-1}}{\dot{e}_{i1}^{(p_i/q_i)-1} - \eta_i} \hat{\varepsilon}_i + |s_i| \varepsilon_i - \frac{1}{\tau_i} \widetilde{\varepsilon}_i \dot{\hat{\varepsilon}}_i \\
& - |s_i| \frac{\dot{e}_{i1}^{(p_i/q_i)-1}}{I\left(\dot{e}_{i1}^{(p_i/q_i)-1} - \eta_i \right)} \hat{\mathbf{W}}_i^T \underline{\zeta}_i(\underline{\mathbf{e}}_i) + |s_i| \underline{\mathbf{W}}_i^{*T} \underline{\zeta}_i(\underline{\mathbf{e}}_i) - \frac{1}{r_i} \widetilde{\mathbf{W}}_{\mathbf{i}}^{\mathbf{T}} \dot{\hat{\mathbf{W}}}_{\mathbf{i}} \Bigg].
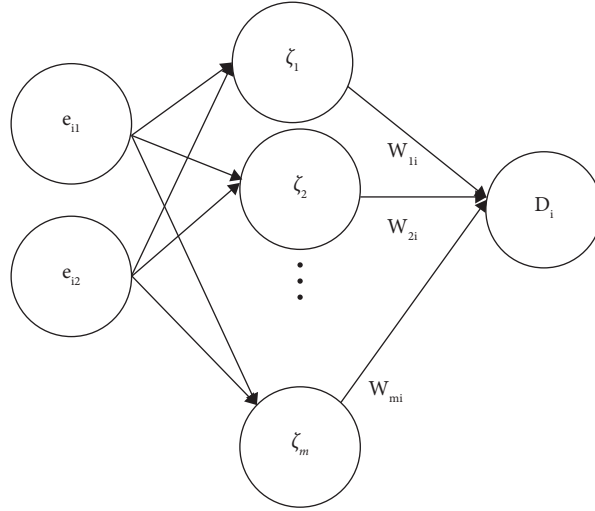\end{aligned}
\tag{27}
$$

FIGURE 2: Neural network learning model.

For $0 \le \dot{e}_{i1}^{(p_i/q_i)-1} < 1$, $|s_i|\underline{\widehat{\mathbf{W}}}_i^T \underline{\zeta}_i(\underline{\mathbf{e}}_i) < |s_i|\dot{e}_{i1}^{(p_i/q_i)-1}\underline{\widehat{\mathbf{W}}}_i^T \underline{\zeta}_i(\underline{\mathbf{e}}_i)$ ≤ 0, and then, $\exists \eta_i > 2$ makes $\dot{e}_{i1}^{(p_i/q_i)-1} - \eta_i \ne 0$, $(\dot{e}_{i1}^{(p_i/q_i)-1}/(\dot{e}_{i1}^{(p_i/q_i)-1} - \eta_i)) \ge -1$.

When $\underline{\widehat{\mathbf{W}}}_i^T \underline{\zeta}_i < 0$, the following results can be obtained by (27):

$$\dot{V} \le \sum_{i=1}^{6}\left[-\frac{p_i}{b_i q_i}\dot{e}_{i1}^{(p_i/q_i)-1}s_i^2 + |s_i|\varepsilon_i - |s_i|\frac{\dot{e}_{i1}^{(p_i/q_i)-1}}{\dot{e}_{i1}^{(p_i/q_i)-1} - \eta_i}\widehat{\varepsilon}_i - \frac{1}{\tau_i}\widetilde{\varepsilon}_i\dot{\widehat{\varepsilon}}_i \right.$$

$$\left. + |s_i|\underline{\mathbf{W}}_i^{*T}\underline{\zeta}_i(\underline{\mathbf{e}}_i) - |s_i|\underline{\widehat{\mathbf{W}}}_i^T\underline{\zeta}_i(\underline{\mathbf{e}}_i) - \frac{1}{r_i}\widetilde{\mathbf{W}}_{\mathbf{i}}^{\mathbf{T}}\dot{\widehat{\mathbf{W}}}_{\mathbf{i}} \right] \tag{28}$$

$$\le \sum_{i=1}^{6}\left[-\frac{p_i}{b_i q_i}\dot{e}_{i1}^{(p_i/q_i)-1}s_i^2 + |s_i|\widetilde{\varepsilon}_i - \frac{1}{\tau_i}\widetilde{\varepsilon}_i\dot{\widehat{\varepsilon}}_i + |s_i|\widetilde{\mathbf{W}}_{\mathbf{i}}^{\mathbf{T}}\underline{\zeta}_i(\underline{\mathbf{e}}_i) - \frac{1}{r_i}\widetilde{\mathbf{W}}_{\mathbf{i}}^{\mathbf{T}}\dot{\widehat{\mathbf{W}}}_{\mathbf{i}} \right].$$

When $\underline{\widehat{\mathbf{W}}}_i^T \underline{\zeta}_i \ge 0$, the following results can be obtained by (27):

$$\dot{V} \le \sum_{i=1}^{6}\left[-\frac{p_i}{b_i q_i}\dot{e}_{i1}^{(p_i/q_i)-1}s_i^2 - |s_i|\frac{\dot{e}_{i1}^{(p_i/q_i)-1}}{\dot{e}_{i1}^{(p_i/q_i)-1} - \eta_i}\widehat{\varepsilon}_i + |s_i|\varepsilon_i - \frac{1}{\tau_i}\widetilde{\varepsilon}_i\dot{\widehat{\varepsilon}}_i \right.$$

$$\left. - |s_i|\frac{\dot{e}_{i1}^{(p_i/q_i)-1}}{I\left(\dot{e}_{i1}^{(p_i/q_i)-1} - \eta_i\right)}\widehat{\mathbf{W}}_i^T\underline{\zeta}_i(\underline{\mathbf{e}}_i) + |s_i|\underline{\mathbf{W}}_i^{*T}\underline{\zeta}_i(\underline{\mathbf{e}}_i) - \frac{1}{r_i}\widetilde{\mathbf{W}}_{\mathbf{i}}^{\mathbf{T}}\dot{\widehat{\mathbf{W}}}_{\mathbf{i}} \right]$$

$$\le \sum_{i=1}^{6}\left[-\frac{p_i}{b_i q_i}\dot{e}_{i1}^{(p_i/q_i)-1}s_i^2 + |s_i|\varepsilon_i - \frac{\dot{e}_{i1}^{(p_i/q_i)-1}}{\dot{e}_{i1}^{(p_i/q_i)-1} - \eta_i}|s_i|\widehat{\varepsilon}_i - \frac{1}{\tau_i}\widetilde{\varepsilon}_i\dot{\widehat{\varepsilon}}_i \right.$$

$$+ |s_i| \underline{\mathbf{W}}_i^{*T} \underline{\boldsymbol{\zeta}}_i (\mathbf{e}_i) - \frac{\dot{e}_{i1}^{(p_i/q_i)-1}}{\dot{e}_{i1}^{(p_i/q_i)-1} - \eta_i} |s_i| \widehat{\mathbf{W}}_i^T \underline{\boldsymbol{\zeta}}_i (\mathbf{e}_i) - \frac{1}{r_i} \widetilde{\underline{\mathbf{W}}}_{\mathbf{i}}^{\mathbf{T}} \dot{\widehat{\mathbf{W}}}_{\mathbf{i}} \Bigg]$$

$$\leq \sum_{i=1}^{6} \Bigg[-\frac{p_i}{b_i q_i} \dot{e}_{i1}^{(p_i/q_i)-1} s_i^2 + |s_i| \widetilde{\varepsilon}_i - \frac{1}{\tau_i} \widetilde{\varepsilon}_i \dot{\widehat{\varepsilon}}_i + |s_i| \widetilde{\underline{\mathbf{W}}}_{\mathbf{i}}^{\mathbf{T}} \underline{\boldsymbol{\zeta}}_i (\mathbf{e}_i)$$

$$- \frac{1}{r_i} \widetilde{\underline{\mathbf{W}}}_{\mathbf{i}}^{\mathbf{T}} \dot{\widehat{\mathbf{W}}}_{\mathbf{i}} \Bigg].$$

$$(29)$$

When the first line of (15) and (16) is established, the following results can be obtained by (28) and (29):

$$\dot{V} \leq \sum_{i=1}^{6} \Bigg[-\frac{p_i}{b_i q_i} \dot{e}_{i1}^{(p_i/q_i)-1} s_i^2 + |s_i| \widetilde{\varepsilon}_i - \frac{1}{\tau_i} \widetilde{\varepsilon}_i \dot{\widehat{\varepsilon}}_i$$

$$+ |s_i| \widetilde{\underline{\mathbf{W}}}_{\mathbf{i}}^{\mathbf{T}} \underline{\boldsymbol{\zeta}}_i (\mathbf{e}_i) - \frac{1}{r_i} \widetilde{\underline{\mathbf{W}}}_{\mathbf{i}}^{\mathbf{T}} \dot{\widehat{\mathbf{W}}}_{\mathbf{i}} \Bigg] \qquad (30)$$

$$\leq \sum_{i=1}^{6} \left(-\frac{p_i}{b_i q_i} \dot{e}_{i1}^{(p_i/q_i)-1} s_i^2 \right).$$

When the second line of (15) and (16) is established, the following results can be obtained by (28) and (29):

$$\dot{V} \leq \sum_{i=1}^{6} \Bigg[-\frac{p_i}{b_i q_i} \dot{e}_{i1}^{(p_i/q_i)-1} s_i^2 + |s_i| \widetilde{\varepsilon}_i - \frac{1}{\tau_i} \widetilde{\varepsilon}_i \dot{\widehat{\varepsilon}}_i + |s_i| \widetilde{\underline{\mathbf{W}}}_{\mathbf{i}}^{\mathbf{T}} \underline{\boldsymbol{\zeta}}_i (\mathbf{e}_i) - \frac{1}{r_i} \widetilde{\underline{\mathbf{W}}}_{\mathbf{i}}^{\mathbf{T}} \dot{\widehat{\mathbf{W}}}_{\mathbf{i}} \Bigg]$$

$$\leq \sum_{i=1}^{6} \left(-\frac{p_i}{b_i q_i} \dot{e}_{i1}^{(p_i/q_i)-1} s_i^2 + |s_i| \left| \frac{\widetilde{\varepsilon}_i \widehat{\varepsilon}_i \widehat{\varepsilon}_i}{\|\widehat{\varepsilon}_i\|^2} \right| + |s_i| \frac{\widetilde{\mathbf{W}}_i^T \widehat{\mathbf{W}}_i \widehat{\mathbf{W}}_i^T}{\|\widehat{\mathbf{W}}_i\|^2} \underline{\boldsymbol{\zeta}}_i (\mathbf{e}_i) \right),$$

$$(31)$$

where $\| \widehat{\mathbf{W}}_i \| = M_{W_i}, \| \mathbf{W}_i^* \| \leq M_{W_i}, \| \mathbf{W}_i^* - \widehat{\mathbf{W}}_i \| \leq M_{W_i}.$ $|\widehat{\varepsilon}_i| = M_{\widehat{\varepsilon}_i}, |\varepsilon_i| \leq M_{\widehat{\varepsilon}_i}, |\widehat{\varepsilon}_i - \varepsilon_i| \leq M_{\widehat{\varepsilon}_i}.$

Therefore,

$$\widetilde{\underline{\mathbf{W}}}_i^T \widehat{\mathbf{W}}_i = \frac{\left\| \mathbf{W}_i^* \right\|^2 - \left\| \widehat{\mathbf{W}}_i \right\|^2 - \left\| \underline{\mathbf{W}}_i^* - \widehat{\mathbf{W}}_i \right\|^2}{2} \leq 0, \qquad (32.1)$$

$$\widetilde{\varepsilon}_i \widehat{\varepsilon}_i = \frac{\varepsilon_i^2 - \widehat{\varepsilon}_i^2 - (\varepsilon_i - \widehat{\varepsilon}_i)^2}{2} \leq 0, \qquad (32.2)$$

and the following results can be obtained by (30)–(32):

$$\dot{V} \leq \sum_{i=1}^{6} \left(-\frac{p_i}{b_i q_i} \dot{e}_{i1}^{(p_i/q_i)-1} s_i^2 \right)$$

$$\leq \sum_{i=1}^{6} \Bigg[-\frac{2p_i}{b_i q_i} \dot{e}_{i1}^{(p_i/q_i)-1} \times \left(\frac{s_i^2}{2} + \frac{1}{2r_i} \widetilde{\underline{\mathbf{W}}}_{\mathbf{i}}^{\mathbf{T}} \dot{\widehat{\mathbf{W}}}_{\mathbf{i}} + \frac{1}{2\tau_i} \widetilde{\varepsilon}_i^2 \right)$$

$$+ \frac{2p_i}{b_i q_i} \dot{e}_{i1}^{(p_i/q_i)-1} \left(\frac{1}{2r_i} \widetilde{\underline{\mathbf{W}}}_{\mathbf{i}}^{\mathbf{T}} \dot{\widehat{\mathbf{W}}}_{\mathbf{i}} + \frac{1}{2\tau_i} \widetilde{\varepsilon}_i^2 \right) \Bigg]$$

$$\leq \sum_{i=1}^{6} \left(-\frac{p_i}{b_i q_i} \dot{e}_{i1}^{(p_i/q_i)-1} V_i \right) + \sum_{i=1}^{6} \frac{p_i}{b_i q_i r_i} \left(M_{W_i}^2 + M_{\varepsilon_i}^2 \right)$$

$$\leq - \min_{i=1,2,3,4,5,6} \left(\frac{p_i}{b_i q_i} \dot{e}_{i1}^{(p_i/q_i)-1} \right) \sum_{i=1}^{6} V_i + \sum_{i=1}^{6} \frac{p_i}{b_i q_i r_i} \left(M_{W_i}^2 + M_{\varepsilon_i}^2 \right)$$

$$\leq - mV + L.$$

$$(33)$$

Here, $m = \min_{i=1,2,3,4,5,6}((p_i/b_iq_i)\dot{e}_{i1}^{(p_i/q_i)-1})$, $L = \sum_{i=1}^{6}(p_i/b_iq_ir_i)(M_{W_i}^2 + M_{\varepsilon_i}^2)$.

We know V is bounded from inequality (33) and the results in literature [20, 21], and s_i convergence to 0 is achieved exponentially.

We suppose that $t = t_1$ when the subsystem reaches the sliding mode surface, i.e., $s_i = 0$. When $t > t_1$, the dynamic equation of tracking error of the first subsystem obtained by equation (11) is given by

$$\dot{e}_{i1} = -e_{i1}^{(q_i/p_i)} \cdot b_i^{(q_i/p_i)}\left(1 + \frac{1}{a_i}e_{i1}^{(k_i/h_i)-1}\right)^{(q_i/p_i)}. \qquad (34)$$

We deform (34) to (35) as follows:

$$\left(\frac{1}{e_{i1}}\right)^{(q_i/p_i)} de_{i1} = -b_i^{(q_i/p_i)}\left(1 + \frac{1}{a_i}e_{i1}^{(k_i/h_i)-1}\right)^{(q_i/p_i)} dt. \qquad (35)$$

Derivatives on both sides of (35) can obtain

$$\int_{e_{i1}(t_1)}^{e_{i1}(t_1+\Delta t)}\left(\frac{1}{e_{i1}}\right)^{q_i/p_i} de_{i1} = -\int_{t_1}^{t_1+\Delta t} b_i^{q_i/p_i}\left(1 + \frac{1}{a_i}e_{i1}^{k_i/h_i-1}\right)^{q_i/p_i} dt$$

$$\leq -\int_{t_1}^{t_1+\Delta t} b_i^{k_i/h_i} dt. \qquad (36)$$

The following results can be obtained by (36):

$$e_{i1}^{(p_i-q_i)/p_i}(t_1 + \Delta t) \leq e_{i1}^{(p_i-q_i)/p_i}(t_1) - \frac{p_i - q_i}{p_i}b_i^{(q_i/p_i)}\Delta t, \qquad (37)$$

p_i, q_i are all positive and odd numbers, and $1 < p_i/q_i < 2$, and then, $(p_i - q_i)/p_i > 0$. e_{i1} is in the process of convergence to 0; i.e., $e_{i1} < 1$, $e_{i1}^{(p_i-q_i)/p_i}(t_1 + \Delta t)$ decreases monotonically as Δt grows. It is assumed that the subsystem converges to 0 after reaching the sliding mode surface for t_s time, i.e., $e_{i1}^{(p_i-q_i)/p_i}(t_1 + t_s) = 0$. Thus,

$$t_s \leq \frac{(1/b_i)^{q_i/p_i}p_i}{p_i - q_i}e_{i1}^{1-q_i/p_i}(t_1). \qquad (38)$$

In summary, the tracking error e_{i1} of the $i-$th$(i = 1\cdots 6)$ subsystem can then converge rapidly to zero in finite-time t_s.

5. Simulation Results and Discussion

To verify the effectiveness of the nonsingular fast terminal sliding mode neural network decentralized control (FTSMNNDC) method designed for the quadrotor UAV described in (1), this section will then test the control algorithm by simulation based on the numerical analysis method. The number of neurons in the hidden layer of the neural network is 6, and the j-th neuron basis function center and the base width parameter are taken as

$$\sigma_{ij} = c_{ij} = 0.05, \quad (i = 1, 2\cdots 6, j = 1, 2\cdots 6). \qquad (39)$$

The physical parameters of the quadrotor UAV are shown in Table 1 [14]. The settings of the position, posture,

TABLE 1: Parameters of the quadrotor UAV.

Parameters	Numeric values
M	1.1 kg
G	$9.81\ s^{-2}\cdot$ m
l	0.21 m
$I_x = I_y$	0.022 Ns^2/rad
I_z	0.022 Ns^2/rad
J_r	0.02 Ns^2/rad
$l_1 = l_2 = l_3$	0.001 Ns/m
$l_4 = l_5 = l_6$	0.0012 Ns/m
B	5 Ns^2
D	9×10^{-2} Ns^2

TABLE 2: Initial position and attitude values of the quadrotor UAV and their respective reference tracks and angles.

Parameters	Numeric values
$x(0)(x_{11}(0))$	0 m
$\dot{x}(0)(\dot{x}_{12}(0))$	0 m/s
$\varphi(0)(x_{41}(0))$	0°
$x_d(y_{d1})$	$0.5\sin(0.5t)$m
ψ_d	$15°\sin(0.5t)$
$y(0)(x_{21}(0))$	0 m
$\dot{y}(0)(\dot{x}_{22}(0))$	0 m/s
$\theta(0)(x_{51}(0))$	0°
$y_d(y_{d2})$	$0.5\cos(0.5t)$m
θ_d	$15°\sin(0.5t)$
$z(0)(x_{31}(0))$	0 m
$\dot{z}(0)(\dot{x}_{32}(0))$	0 m/s
$\gamma(0)(x_{61}(0))$	0°
$z_d(y_{d3})$	$\begin{cases}(t+1)\text{m}, & \text{when } z_d \leq Y_{d3}, \\ (-t+2Y_{d3})\text{m}, & \text{when } z_d > Y_{d3}.\end{cases}$
γ_d	$15°\sin(0.5t)$

TABLE 3: External disturbances and torques.

Parameters	Numeric values
$d_1(t)$	$-0.04[1 + \sin(0.3\pi t)]$N
$d_2(t)$	$0.024[1 + \sin(0.3\pi t)]$N
$d_3(t)$	$-0.024[1 + \sin(0.3\pi t)]$N
$d_4(t)$	$-I_x[1 + \sin(0.2\pi t)]$N·m
$d_5(t)$	$I_y[1 + \sin(0.2\pi t)]$N·m
$d_6(t)$	$-2I_z[1 + \sin(0.2\pi t)]$N·m

TABLE 4: Relevant parameters of the controller and the adaptive laws of the parameters $(i = 1\cdots 6)$.

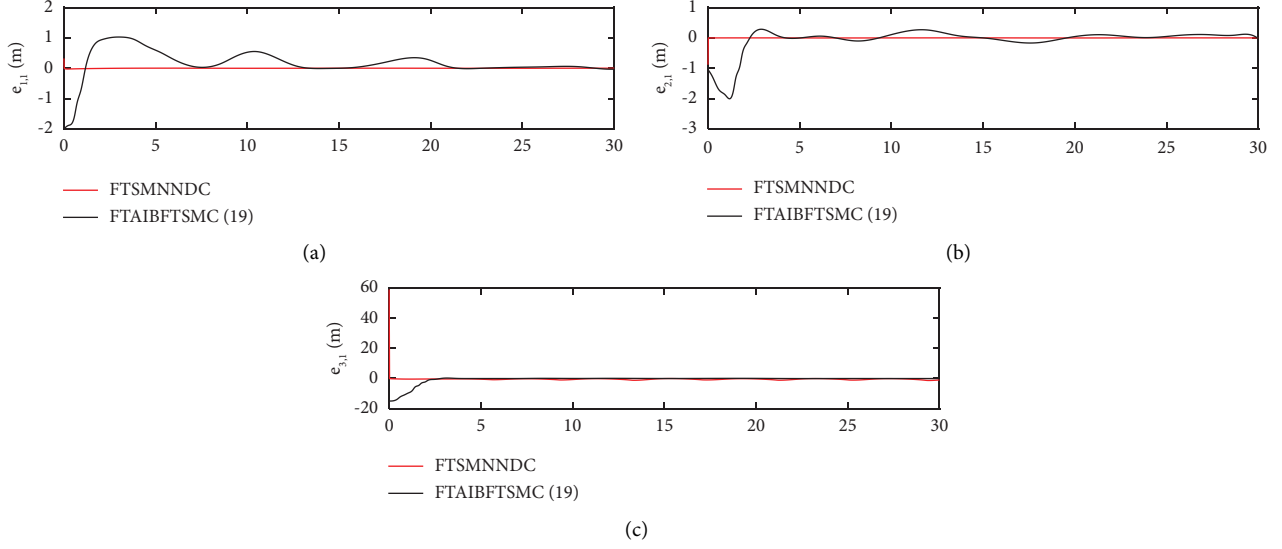| Parameters	Numeric values
k_i	5
Y_{di}	$\begin{cases}0.5\ (i = 1, 2, 4, 5, 6), \\ 10\ (i = 3),\end{cases}$
r_i	0.1
h_i	3
η_i	3
τ_i	0.1
p_i	11
a_i	0.2
M_{Wi}	1
q_i	9
b_i	0.25
$M_{\varepsilon i}$	1

(a)

(b)

(c)

Figure 3: Position-tracking error response curves: (a) tracking error in the x axis; (b) tracking error in the y axis; (c) tracking error in the z axis.
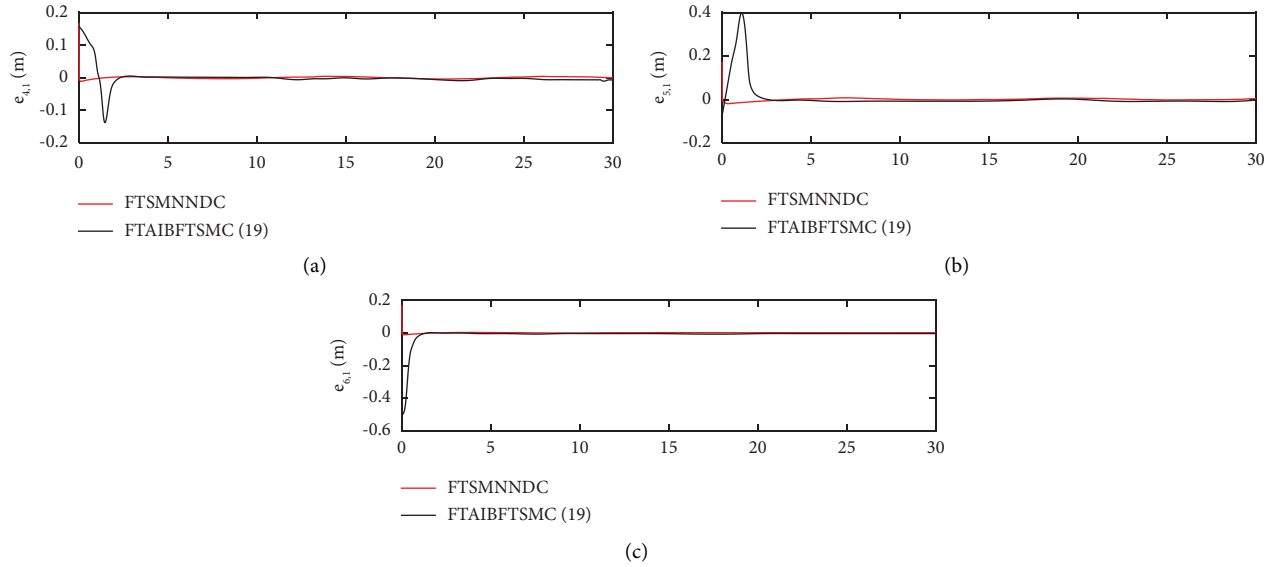

(a)

(b)

(c)

Figure 4: Attitude-tracking error response curves: (a) tracking error of the pitch angle; (b) tracking error of the roll angle; (c) tracking error of the yaw angle.

attitude, and reference heading angle are shown in Table 2 [9]; considering that the altitude of UAV flight is limited, the trajectory of $z_d(y_{d3})$ is optimized on the basis of literature [9] as follows:

$$z_d(y_{d3}) = \begin{cases} t + 1, & \text{when } z_d \leq Y_{d3}, \\ -t + 2Y_{d3}, & \text{when } z_d > Y_{d3}, \end{cases} \tag{40}$$

where the constant $Y_{d3} > 0$ is the highest flight altitude that the drone can reach. External unknown perturbations are shown in Table 3 [9], and the relevant parameters of the designed controller and parameter adaptive laws are shown in Table 4.

In order to verify that the designed decentralized control method has better performance, the nonsingular fast terminal sliding mode neural network decentralized control (FTSMNNDC) method and finite-time adaptive integral backstepping fast terminal sliding mode control (FT-AIBFTSMC) method proposed by literature [17] are compared for simulation analysis.

Figures 3 and 4 show the three-channel position tracking error response curves and the three-channel attitude angle tracking error response curves of the quadrotor UAV under two different control methods, respectively. The comparative analysis of two different control methods is conducted from two aspects:
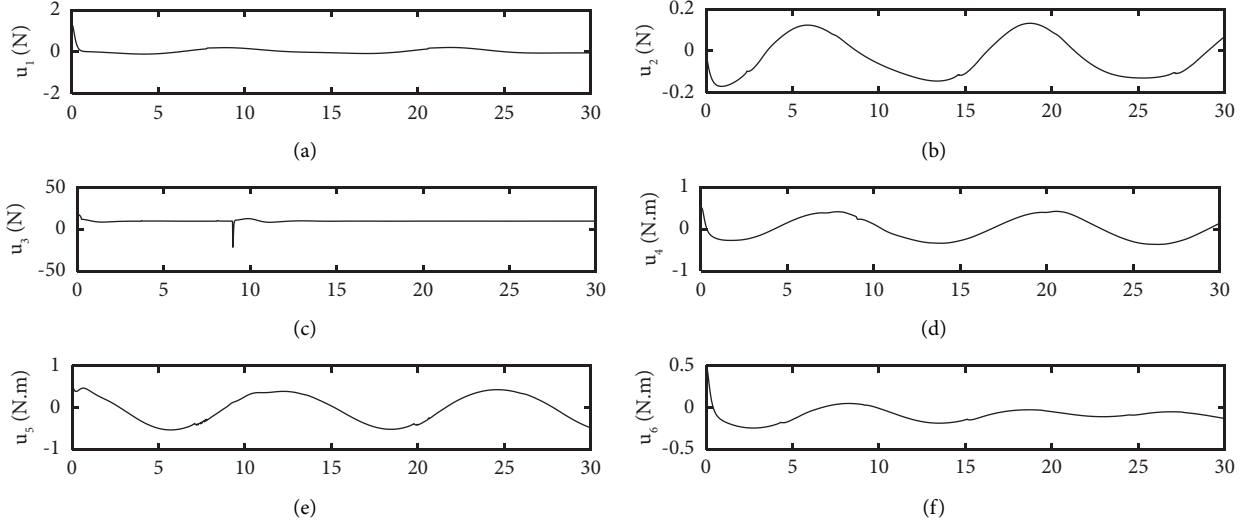
FIGURE 5: Position and attitude virtual decentralized controllers: (a) virtual decentralized controller of the x-axis; (b) virtual decentralized controller of the y-axis; (c) virtual decentralized controller of the z-axis; (d) virtual decentralized controller of the pitch attitude; (e) virtual decentralized controller of the roll attitude; (f) virtual decentralized controller of the yaw attitude.
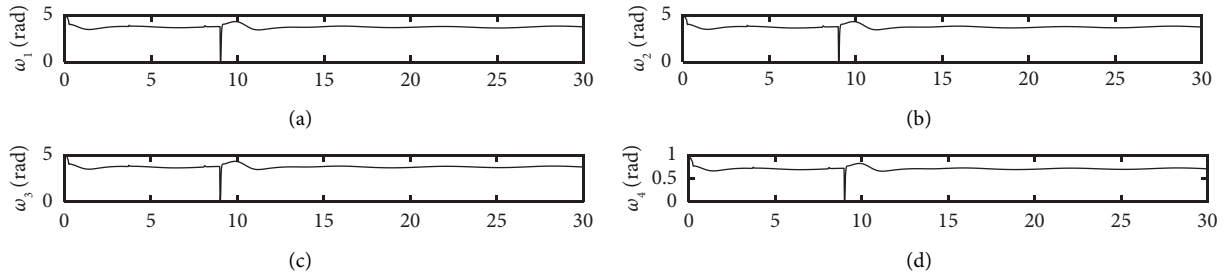

FIGURE 6: The angular velocity response curves of each propeller: (a) the angular speed of the first propeller; (b) the angular speed of the second propeller; (c) the angular speed of the third propeller; (d) the angular speed of the fourth propeller.

(1) Tracking speed: Although both methods can track the desired track for a limited time, it is clear that the proposed method is much faster than the literature [17] method. In this paper, we have proved that e_{i1} is in the process of convergence to 0, i.e., $e_{i1} < 1$. From formula (38), we can obtain that as long as

$$b_i \geq \left(\frac{p_i - q_i}{p_i} \right)^{-(p_i/q_i)} . \tag{41}$$

Then,

$$t_s \leq \frac{(1/b_i)^{(p_i/q_i)} p_i}{p_i - q_i} e_{i1}^{(1-(p_i/q_i))} (t_1) < 1. \tag{42}$$

So the three position variables and the three attitude variables can effectively track the desired track within 1 s. Indeed, since e_{i1} is close to 0, $e_{i1}^{1-p_i/q_i}(t_1)$ is much less than 1; therefore, t_s is much less than 1, and the tracking error converges to 0 almost instantly. The simulation results also confirm this conclusion very well. While simulation conclusions in [16] show that the fastest tracking speed of

literature [17] is close to 5 s, the slowest tracking speed is nearly 30 s.

(2) Tracking effect: Both methods have a good tracking effect, and both can ensure that the tracking error is close to zero, but the proposed method of this paper is more stable.

Figure 5 shows the quadrotor position and attitude virtual decentralized controller and the resulting total lift, rolling torque, pitch torque, and yaw torque. In simulation, the controllers are chosen by formula (14), whose parameters are given in Table 4.

Figure 6 shows the control inputs for the actual angular velocity of the four propellers obtained by mapping equation (2). It can be seen that the actual control inputs of both the virtual decentralized controller and the actual control inputs of the propellers are bounded, which meet the requirements of the actual control task.

6. Conclusion

This paper designs the attitude decentralized controller and the position virtual decentralized controller for the strongly coupled and insufficient driven quadrotor UAV which is

disturbed by the external wind field. It reduces the control complexity caused by external interference and the coupling of the system itself and improves the control performance of the controller. By making a comprehensive use of the nonsingular fast terminal sliding mode technique and the neural network approximation technique, we accelerate the trajectory-tracking speed of the controller and enable the proposed controller to quickly track the desired trajectories. The simulation results not only show the effectiveness of the proposed control scheme but also show the faster and more accurate tracking performance by comparing with the existing research results.

In the next step, we will further study the design of effective controllers if the quadrotor actuator is limited or the UAV attitude and track state cannot be observed.

Abbreviations

$E_O(e_x, e_y, e_z)$:	The ground frame
$O(x, y, z)$:	The body frame
x, y, z:	Displacement of the UAV during a horizontal forward, horizontal right, and vertical upward movement, m
$\dot{x}, \dot{y}, \dot{z}$:	First derivative of x, y, z, m/s
$\ddot{x}, \ddot{y}, \ddot{z}$:	Second derivative of x, y, z, m/s^2
φ, θ, ψ:	The roll, pitch, and yaw angles
$\dot{\varphi}, \dot{\theta}, \dot{\psi}$:	First derivative of φ, θ, ψ
$\ddot{\varphi}, \ddot{\theta}, \ddot{\psi}$:	Second derivative of φ, θ, ψ
$\omega_1, \omega_2, \omega_3, \omega_4$:	The rotation speeds of the four rotors, rad/s
b:	The lift coefficient of the rotor
$F_i = b\omega_i^2 (i = 1 \cdots 4)$:	The four lifts provided by the four rotors, N
$q(x, y, z)$:	The corresponding position in the body coordinate system of the UAV when flying
u_h:	Vertical upward control law of the total lift of the body, N
$u_\varphi, u_\theta, u_\psi$:	Rolling moment, pitch moment, and yaw moment inputs, N
u_1, u_2, u_3:	The position decentralized virtual controllers, N
u_4, u_5, u_6:	The attitude decentralized controllers, N.m
$\Delta_i (i = 1 \cdots 6)$:	The total coupling terms of each subsystem composed of external perturbations, model uncertainty, and strong coupling terms between the subsystems
m:	Total mass of UAV, kg
I_x, I_y, I_z:	The moment of inertia of the three axes, Ns^2/rad
J_r:	Propeller inertia, Ns^2/rad
$l_i > 0 \quad (i = 1 \cdots 6)$:	The drag coefficients, Ns/m
$d_i(t), (i = 1 \cdots 6)$:	The external unknown time-varying perturbations, N $(i = 1 \cdots 3)$, N.m $(i = 4 \cdots 6)$
l:	The distance from the center of the drone to the center of the rotor, m
$\mathbf{x}_1 = (x_{11}, x_{21}, x_{31}, x_{41}, x_{51}, x_{61})^T$ $= (x, y, z, \varphi, \theta, \psi)^T$:	States corresponding to the six subsystems, represented by six-dimensional vectors
$\mathbf{x}_2 = (x_{12}, x_{22}, x_{32}, x_{42}, x_{52}, x_{62})^T$ $= (\dot{x}, \dot{y}, \dot{z}, \dot{\varphi}, \dot{\theta}, \dot{\psi})^T$:	The first derivative of the subsystem vector
$\underline{\mathbf{d}} = (d_1, d_2, d_3, d_4, d_5, d_6)^T$:	The external time-varying disturbance of the subsystem
$\mathbf{Y}_d = (y_{d1}, y_{d2}, y_{d3}, y_{d4}, y_{d5}, y_{d6})^T$ $= (x_d, y_d, z_d, \varphi_d, \theta_d, \psi_d)^T$:	The expected tracking trajectory of each subsystem
$\underline{\mathbf{e}}_i = (e_{i1}, e_{i2})^T$:	The trajectory-tracking error of each subsystem of the quadrotor UAV
s_i:	The nonsingular sliding mode surface of each subsystem
$a_i, b_i, k_i, h_i, p_i, q_i$:	Sliding mode surface parameters
c_{ijk}:	Coefficients of the quadratic function
Y_{di}:	Upper bound for tracking traces and their first and second derivatives
sgn ():	The symbolic function
sat ():	The saturation function
$\underline{\mathbf{W}}_i^* = (\mathbf{w}_{1i}, \mathbf{w}_{2i}, \cdots, \mathbf{w}_{mi})^T$:	The optimal weight of the neural network
$\widehat{\underline{\mathbf{W}}}_i$:	The estimate of $\underline{\mathbf{W}}_i^*$
$\widetilde{\underline{\mathbf{W}}} = \underline{\mathbf{W}}_i^* - \widehat{\underline{\mathbf{W}}}$:	Estimation error of the neural network weights
$\boldsymbol{\zeta}_i(\underline{\mathbf{e}}_i)$:	The basis function vector of the neural network
$\zeta_{ij}(\underline{\mathbf{e}}_i)$:	Basis functions
σ_{ij}, c_{ij}:	Center and basis width parameters of the j-th neuron basis function in the hidden layer
$\varepsilon_i(\underline{\mathbf{e}}_i)$:	The approximation errors of the neural network
ε_i:	Upper bound for the neural network approximation error
$\widehat{\varepsilon}_i$:	The estimates of ε_i
$\widetilde{\varepsilon}_i$:	Estimation error for the upper bound of the neural network approximation error
r_i, τ_i:	The parametric adaptive rates of the neural network weights and approximation error
$M_{W_i}, M_{\widehat{\varepsilon}_i}, \eta_i, I$:	The design constants.

Data Availability

No data were used to support this study.

Additional Points

The parameters of UAV refer to the parameters commonly used in the existing research literature. The initial value of neural network approximation and the design parameters of the system are selected within the conditions of the design of the controller.

Conflicts of Interest

The authors declare that they have no conflicts of interest.

Acknowledgments

References

[1] H. Heidari and M. Saska, "Trajectory planning of quadrotor systems for various objective functions," *Robotica*, vol. 39, no. 1, pp. 137–152, 2021.

[2] H. Ma, M. Chen, G. Feng, and Q. Wu, "Disturbance-observer-based adaptive fuzzy tracking control for unmanned autonomous helicopter with flight boundary constraints," *IEEE Transactions on Fuzzy Systems*, vol. 31, no. 1, pp. 184–198, 2023.

[3] T. Manzoor, H. Pei, and Z. Cheng, "Composite observer-based robust model predictive control technique for ducted fan aerial vehicles," *Nonlinear Dynamics*, vol. 111, no. 4, pp. 3433–3450, 2023.

[4] F. Ma, Z. Yang, and P. Ji, "Sliding mode controller based on the extended state observer for plant-protection quadrotor unmanned aerial vehicles," *Mathematics*, vol. 10, no. 8, p. 1346, 2022.

[5] M. Ashraf, E. Safwat, A. M. Kamel, and M. A. H. Abozied, "Design and analysis of A nonlinear flight control law based on extended state observer," in *Proceedings of the 2022 International Telecommunications Conference (ITC-Egypt)*, pp. 26–28, Alexandria, Egypt, July 2022.

[6] J. Liang, Y. Chen, N. Lai, and B. He, "Robust observer-based trajectory tracking control for unmanned aerial manipulator," *International Journal of Control, Automation, and Systems*, vol. 21, no. 2, pp. 616–629, 2023.

[7] T.-N. Ma, R.-D. Xi, X. Xiao, and Z.-X. Yang, "Nonlinear extended state observer based prescribed performance control for quadrotor UAV with attitude and input saturation constraints," *Machines*, vol. 10, no. 7, p. 551, 2022.

[8] M. B. Mohiuddin and A. M. Abdallah, "Dynamic modeling and control of quadrotor slung-load system using PID and nonlinear backstepping controller," *AIAA Scitech*, vol. 18, 2021.

[9] Y. Zhang, Z. Chen, and M. Sun, "Trajectory tracking control for a quadrotor unmanned aerial vehicle based on dynamic surface active disturbance rejection control," *Transactions of the Institute of Measurement and Control*, vol. 42, no. 12, pp. 2198–2205, 2020.

[10] Z. Zhao, D. Cao, J. Yang, and H. Wang, "High-order sliding mode observer-based trajectory tracking control for a quadrotor UAV with uncertain dynamics," *Nonlinear Dynamics*, vol. 102, no. 4, pp. 2583–2596, 2020.

[11] C. Zhang, G. Zhang, and Q. Dong, "Adaptive dynamic programming-based adaptive-gain sliding mode tracking control for fixed-wing unmanned aerial vehicle with disturbances," *International Journal of Robust and Nonlinear Control*, vol. 33, no. 2, pp. 1065–1097, 2022.

[12] O. Mechali, L. Xu, X. Xie, and J. Iqbal, "Fixed-time nonlinear homogeneous sliding mode approach for robust tracking control of multirotor aircraft: experimental validation," *Journal of the Franklin Institute*, vol. 359, no. 5, pp. 1971–2029, 2022.

[13] P. Gao, G. Wang, Y. Ji et al., "Event-triggered tracking control scheme for quadrotors with external disturbances: theory and validations," in *Proceedings of the 2022 IEEE International Conference on Robotics and Automation (ICRA)*, Philadelphia, PA, USA, May, 2022.

[14] F. Serrano, O. Castillo, M. Alassafi, F. Alsaadi, and A. Ahmad, "Terminal sliding mode attitude-position quaternion based control of quadrotor unmanned aerial vehicle," *Advances in Space Research*, vol. 71, no. 9, pp. 3855–3867, 2023.

[15] M. Omar, L. Xu, Y. Huang, M. Shi, and X. Xie, "Observer-based fixed-time continuous nonsingular terminal sliding mode control of quadrotor aircraft under uncertainties and disturbances for robust trajectory tracking: theory and experiment," *Control Engineering Practice*, vol. 111, 2021.

[16] F. Qian, P. Mao, L. Shen, and J. Wang, "A global fast terminal sliding mode control for trajectory tracking of unmanned aerial manipulation," *Measurement and Control*, vol. 11, pp. 763–776, 2022.

[17] K. Eliker and W. Zhang, "Finite-time adaptive integral backstepping fast terminal sliding mode control application on quadrotor UAV," *International Journal of Control, Automation and Systems*, vol. 18, no. 2, pp. 415–430, 2020.

[18] P. Yang, F. Kejia, Y. Ding, and Z. Shen, "Fast terminal sliding mode control based on finite-time observer and improved reaching law for aerial robots," *Actuators*, vol. 11, no. 9, 258 pages, 2022.

[19] L. Bo, H. Zhang, Y. Niu, D. Ran, and B. Xiao, "Finite-time disturbance observer-based trajectory tracking control for quadrotor unmanned aerial vehicle with obstacle avoidance," *Mathematical Methods in the Applied Sciences*, vol. 36, no. 1, pp. 1096–1110, 2023.

[20] S. S. Ge and C. Wang, "Adaptive neural control of uncertain MIMO nonlinear systems," *IEEE Transactions on Neural Networks*, vol. 15, no. 3, pp. 674–692, 2004.

[21] L. X. Wang, "Stable adaptive fuzzy control of nonlinear systems," *IEEE Transactions on Fuzzy Systems*, vol. 1, no. 2, pp. 146–155, 1993.